THE JOURNAL OF PHYSICAL CHEMISTRY LETTERS
A JOURNAL OF THE AMERICAN CHEMICAL SOCIETY

pubs.acs.org/JPCL

Letter

Non-negligible Axial Ligand Effect on Electrocatalytic CO_2 Reduction with Iron Porphyrin Complexes

Jiancong Zheng, Dexia Zhou, Jinxiu Han, Jing Liu, Rui Cao, Haitao Lei,* Hongtao Bian,* and Yu Fang

Cite This: *J. Phys. Chem. Lett.* 2022, 13, 11811−11817

Read Online

ACCESS | Metrics & More | Article Recommendations | Supporting Information

ABSTRACT: Iron(III) porphyrin complexes have been demonstrated as one of the efficient molecular catalysts for the electrochemical reduction of CO_2. However, the role of axial ligands coordinated with a metal center in the complex on the electrochemical CO_2 reduction activity has not been fully explored yet. Herein, iron(III) tetraphenylporphyrin thiocyanate (FeTPP-SCN) is synthesized from a commercially available catalyst of FeTPP-Cl by a counteranion exchanging reaction. Cyclic voltammetry measurements showed that the catalytic activity of FeTPP-SCN is noticeably suppressed in the DMF solutions. The structural dynamics of the axial ligand in FeTPP-SCN are further examined by the FTIR and ultrafast IR spectroscopies, where the SCN ligand is employed as the local vibrational probe. Vibrational relaxation measurements showed that the reorientational dynamics of SCN ligands was strongly restricted in DMF solution, suggesting that the subtle electrostatic interaction between the ligands and metal center in the complex can have a non-negligible effect on its catalytic activity.

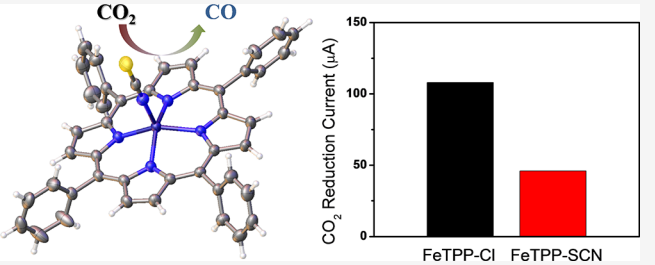

The catalytic reduction of CO_2 has been considered as one of the most practical strategies to solve environmental concerns and future energy demand.[1−4] The development of artificial molecular catalysts for the reduction of CO_2 is the key and has attracted attention from both experimentalist and theoretician in the past few decades.[5−10] Among the molecular catalysts, iron(III) porphyrin complexes are highly efficient and selective for the electrocatalytic conversion of CO_2-to-CO.[11−14] The catalytic activity can be greatly tuned by introduction of the functional substitutes in different sites of the complex, which has been extensively explored in previous reports.[10,15−17] However, the mechanistic studies of solvent and axial ligands effects on the catalytic activity are very limited.[18]

It is generally believed that the axial ligands coordinated with Fe have a negligible effect on the electrochemical CO_2 reduction activity.[19] This is mainly based on the fact that the reaction center is the three-electron-reduced species of Fe^0 or Fe^I, where the axial ligand should be dissociated from the reaction center of the complex. However, the in situ structure and dynamics of the axial ligands in the complex are not fully understood due to the limitations of experimental techniques. The fundamental understanding of structural dynamics of the axial ligands, especially during the electrocatalytic process, would elucidate the underlying mechanism of the electrocatalytic reduction of CO_2 at the molecular level.

Herein, the iron(III) tetraphenylporphyrin thiocyanate (FeTPP-SCN) is synthesized from a commercially available catalyst of FeTPP-Cl by counteranion exchanging reaction, as depicted in Scheme 1. Cyclic voltammetry (CVs) measurements showed that the axial ligand of SCN in FeTPP-SCN can noticeably inhibit the electrocatalytic CO_2 reduction reaction activity in DMF solutions. Linear and nonlinear infrared (IR) spectroscopies are utilized to investigate the structure and dynamics of FeTPP-SCN in DMF solutions. All the measurements revealed that the subtle electrostatic interaction between the axial ligands and metal center in the complex can have non-negligible effect on the electrocatalytic CO_2 reduction.

Figure 1A shows the X-ray crystal structure of synthesized FeTPP-SCN. The detailed crystalline parameters of FeTPP-SCN can be found in Table S1, listed in the Supporting Information. From the crystal structure shown in Figure 1A, the iron(III) atom is coordinated by the porphyrin ligand through four N atoms from pyrroles, which define a square-planar coordination environment. The metal center of the iron(III) atom is further bound to the N atom of thiocyanate ligand to give a five-coordinate square-pyramid geometry. The UV−vis absorption spectrum of FeTPP-SCN in DMF is shown in Figure 1B. Three absorption peaks can be observed at 409, 568, and 609 nm respectively, which are assigned to the Soret and Q bands according to previous studies.[20,21] The NMR data of FeTPP-SCN is also measured and given in Figure S1. All

Received: October 25, 2022
Accepted: December 12, 2022
Published: December 15, 2022

Downloaded via SOUTHERN UNIV SCI & TECHLGY CHINA on February 24, 2025 at 01:44:33 (UTC).
See https://pubs.acs.org/sharingguidelines for options on how to legitimately share published articles.

ACS Publications

© 2022 American Chemical Society

Scheme 1. Counteranion Exchange Reaction from Iron(III) Tetraphenylporphyrin Chloride (FeTPP-Cl) to Iron(III) Tetraphenylporphyrin Thiocyanate (FeTPP-SCN)

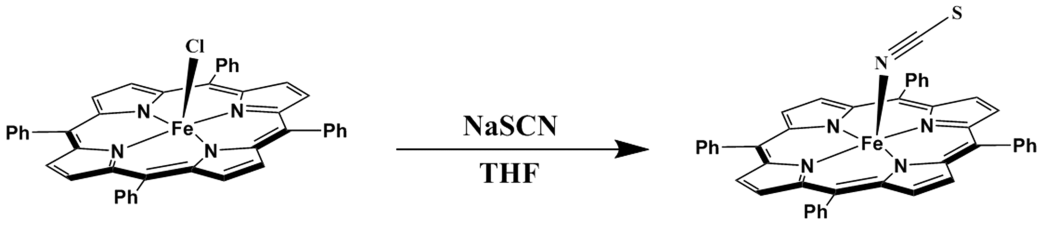

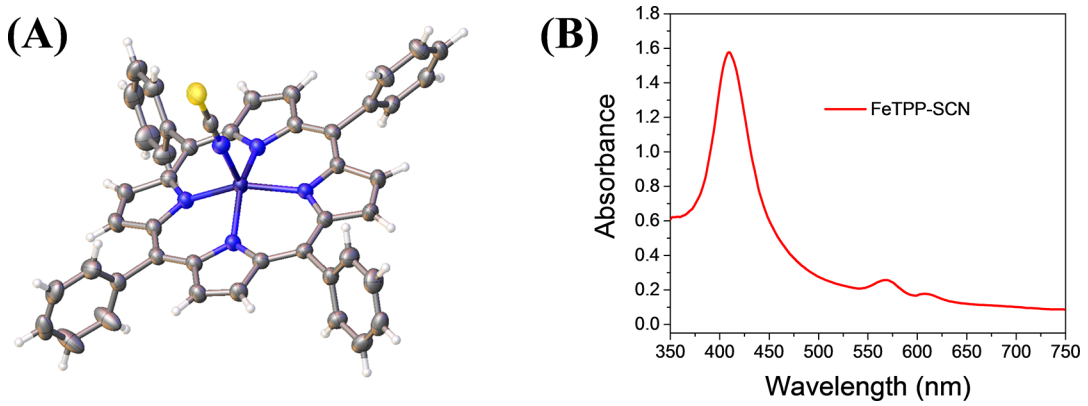

Figure 1. (A) X-ray crystal structure of FeTPP-SCN. Color code: gray, carbon atoms; white, hydrogen atoms; blue, nitrogen atoms; yellow, sulfur atom; black, iron atom. (B) UV−vis absorption spectrum of FeTPP-SCN in DMF. The concentration of FeTPP-SCN was controlled at 2×10^{-5} M.

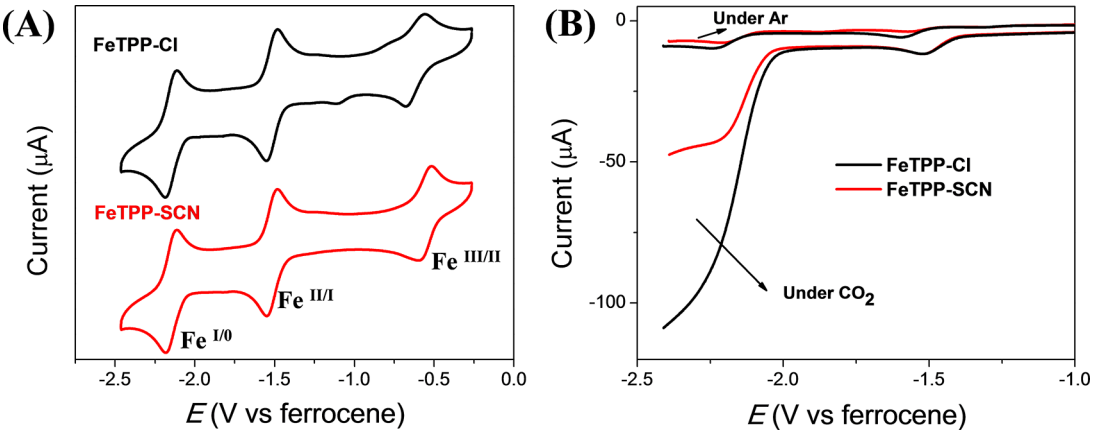

Figure 2. (A) CVs of 0.5 mM FeTPP-SCN and FeTPP-Cl in DMF solutions under Ar (scan rate: 100 mV s^{-1}). The CV curve for FeTPP-Cl in DMF solution is offset for the sake of clarity. (B) Linear sweep voltammetrys of FeTPP-SCN and FeTPP-Cl in DMF under Ar and CO_2 with water as the proton source (both measured at a concentration of 0.28 M H_2O).

these characterization data showed that the electronic structure of the porphyrin scaffold is not affected by the counteranion of thiocyanate.

The CV data of FeTPP-SCN and FeTPP-Cl are both measured in 0.1 M Bu_4NPF_6/DMF solution, shown in Figure 2A. The corresponding three 1e reversible redox waves are assigned to the formal Fe^{III}/Fe^{II}, Fe^{II}/Fe^{I}, and Fe^{I}/Fe^{0} redox couples, respectively. The potentials of these redox couples ($E_{1/2}$) are listed in Table 1. Here, the DMF is chosen as the solvent because of its good solvating properties for both porphyrin complexes and CO_2.[17,22−26] Also the reduction reaction can have a wide potential window in DMF solution. Under argon (Ar), the CV curve of FeTPP-SCN in DMF exhibited three reversible redox waves. The potential of the first redox wave (−0.55 V vs ferrocene) is caused by the Fe^{III}/Fe^{II} redox couple, which was shifted to a more positive potential compared with that of FeTPP-Cl (−0.62 V). The potential difference observed for the first redox wave is generally attributed to the difference of axial ligands. Previous study showed that the first reduction is correlated with the dissociation of the coordinated axial ligands.[27] On the other

Table 1. Reduction Potentials of FeTPP-SCN and FeTPP-Cl in DMF Solutions

	$E_{1/2}$ (V vs ferrocene)		
complex	$Fe^{III/II}$	$Fe^{II/I}$	$Fe^{I/0}$
FeTPP-Cl	−0.62	−1.52	−2.15
FeTPP-SCN	−0.55	−1.52	−2.15

https://doi.org/10.1021/acs.jpclett.2c03235
J. Phys. Chem. Lett. 2022, 13, 11811−11817

side, the Fe^{II}/Fe^{I} (−1.52 V) and Fe^{I}/Fe^{0} (−2.15 V) redox couples were also observed in DMF under Ar and were not affected by the type of axial ligands.

Figure 2B shows the linear sweep voltammetry (LSV) of FeTPP-Cl and FeTPP-SCN under CO_2 in the DMF solution with water as the proton source. It can be found that the $Fe^{I/0}$ redox wave showed a much larger catalytic wave for FeTPP-Cl than that of FeTPP-SCN. Our previous studies demonstrated that this catalytic wave corresponded to the reduction of CO_2, where the Fe^0 was the active species for the CO_2 reduction.[18,28] A control experiment showed that this catalysis was due to the CO_2 rather than the hydrogen evolution reaction, because no such catalytic waves were observed under Ar with same water content, shown in Figure 2B. Furthermore, the intensity of catalytic current increased linearly with a first-order dependence on the concentration of water, shown in Figure S2. The currents of reduction peaks varied linearly with the square root of scan rates, shown in Figure S3, suggesting that both FeTPP-Cl and FeTPP-SCN can diffuse freely in DMF. The Faraday efficiencies for both iron porphyrins are greater than 90%, which indicates that these two substances are excellent molecular catalysts with good stability and selectivity, see Figure S4. The stability of both catalysts was verified by the UV−vis spectroscopic measurements, shown in Figure S5.

The replacement of axial ligands from Cl to SCN can noticeably suppress the electrocatalytic CO_2 reduction reaction activity. Therefore, it is important to investigate the structure and dynamics of the axial ligands in the porphyrin complex dissolved in the DMF solutions. Vibrational spectroscopy is a versatile technique to unravel the structural information by analyzing the specific vibrational modes.[29] Here, the SCN ligands can be served as the vibrational reporter to reveal the structural dynamics in the porphyrin complex by FTIR and nonlinear IR spectroscopies. Ultrafast IR spectroscopy with femtosecond (10^{-15} second) time resolution has been developed as a powerful tool to determine the three-dimensional structure and energy relaxation dynamics in the condensed phases.[29−36]

Figure 3 shows the FTIR spectra in the CN stretching region of FeTPP-SCN and NaSCN dissolved in the DMF solutions.

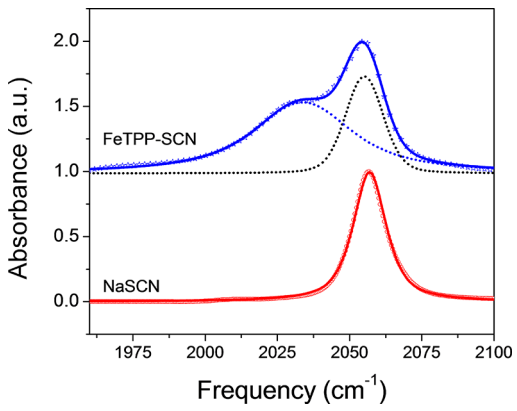

Figure 3. FTIR spectra (in the CN stretching region) of FeTPP-SCN and NaSCN dissolved in DMF solutions, the concentrations were both controlled at 0.02 mol/kg. The background signal was subtracted in the measured FTIR spectra. The FTIR spectrum of FeTPP-SCN is vertically offset for clarification. The solid line is the fitting results by decomposition of the spectrum into two peaks using a pseudo-Voigt function.

Here the thiocyanate anion in the form of Na^+ salt is measured as a control example. It can be found that there is only one absorption peak observed at 2056 cm^{-1} in DMF solution for NaSCN, and it can be assigned to the stretching of CN group.[37] However, there are two absorption peaks in the CN stretching region for FeTPP-SCN in DMF solution, indicating there are two different types of SCN species in the solution. It can be natural to expect that the peak observed at 2055 cm^{-1} would be the free SCN^- dissociated from the metal center of the complex. This assignment is mainly based on the fact that the absorption peak of thiocyanate inorganic salts is positioned at the same frequency in DMF solution.[38] The peak observed at lower frequency of 2033 cm^{-1} is assigned to the bound SCN, where the N atom in SCN ligand should interact with the metal center in the complex. The structure optimization of FeTPP-SCN in the gas phase and with polarizable continuum model was performed by DFT calculation. It was confirmed that the vibrational frequency of CN stretch binding with Fe through a N atom should be shifted to a lower frequency, and the CN stretching frequency for the S-bound type in the complex is shifted to higher frequency than that of isolated SCN. The calibrated frequency of N-bound axial ligand is qualitatively consistent with the experimental observation of 2033 cm^{-1}; see Figure S6 and Table S2.

Another important feature that can be determined from the FTIR measurements is the bandwidth of CN stretches in the complex. The bandwidth (expressed as full-width-at-half-maximum, fwhm) of the bound SCN (~40 cm^{-1}) is much broader than the peak at 2055 cm^{-1} (~15 cm^{-1}). The much broader bandwidth indicates that the bound SCN should experience a dynamically heterogeneous environment. FTIR spectra of FeTPP-SCN in other solvents with lower dielectric constants were also measured, see figure S7. The IR spectroscopic measurements showed that the solvents can affect the vibrational frequency of SCN ligand significantly through controlling the solvent−counteranion interactions.

The structural dynamics of the axial ligands in iron(III) porphyrin complex is further measured by the polarization-dependent ultrafast IR pump−probe experiments, as shown in Figure 4. The narrow-band pump pulse was selected according to the central frequency of SCN ligands, and the fitting parameters for the vibrational relaxation dynamics are listed in Table 2. For the SCN peak at 2055 cm^{-1}, a biexponential decay with time constants of 2.0 ± 0.2 ps (12%) and 15 ± 1 ps (88%) can fit the vibrational population relaxation curve reasonably well. This is quite different from that of free thiocyanate anion dissolved in DMF solution, where its vibrational lifetime is determined to be 46 ± 3 ps.[38] The anharmonicity of SCN band at 2055 cm^{-1} in the porphyrin complex is determined to be ~24 cm^{-1}, which is almost the same as that of the thiocyanate salts dissolved in DMF solution,[38] see Figure S8. The vibrational population relaxation of SCN band is more sensitive to the local environment, as the vibrational energy transfer between these two different SCN species might be occurred.

Furthermore, the reorientational dynamics of SCN ligand (2055 cm^{-1}) showed a biexponential decay behavior, where the fast component of 1.4 ± 0.2 ps (18%) and the slow component of 37 ± 3 ps (82%) were determined accordingly. The fast component is associated with the wobbling motion of the restricted dipole and affected by the solvent molecules.[39−41] The slow component represents the overall orientational relaxation of the porphyrin complex that leads

https://doi.org/10.1021/acs.jpclett.2c03235
J. Phys. Chem. Lett. 2022, 13, 11811−11817

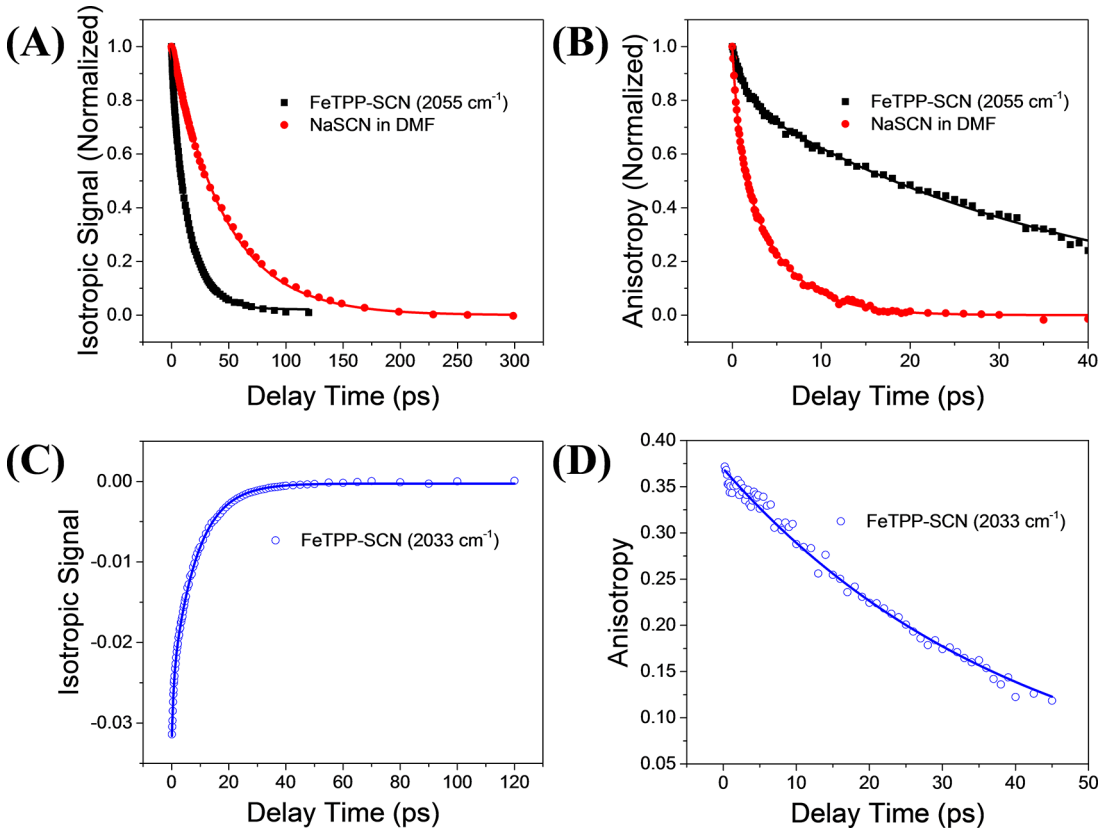

Figure 4. (A) Vibrational population relaxation dynamics for the SCN ligand (2055 cm^{-1}) in the porphyrin complex dissolving in DMF solution. The vibrational population decay of NaSCN dissolving in DMF is also given for comparison. The isotropic signal is determined by analyzing the 0−1 transition of CN stretch with the expression of $P(t) = I_{\parallel}(t) + 2I_{\perp}(t)$. $I_{\parallel}(t)$ and $I_{\perp}(t)$ are the parallel and perpendicular pump−probe signals. (B) Anisotropy decay of SCN stretches in two different systems of FeTPP-SCN and NaSCN. The initial value of anisotropy for both measurements is taken to be 1 for the normalization. The solid lines are the fitting results using biexponential decay function. (C) Vibrational population relaxation dynamics and (D) reorientational dynamics of bound SCN (2033 cm^{-1}) in DMF solutions.

Table 2. Fitting Results for the Vibrational Relaxation Dynamics and Orientational Dynamics of SCN Stretches in FeTPP-SCN and NaSCN Dissolved in DMF Solutions[a]

	population decay (ps)		rotational anisotropy decay (ps)	
samples	T_1	T_2	τ_1	τ_2
FeTPP-SCN in DMF (2055 cm^{-1})	2.0 ± 0.2 (12%)	15 ± 1 (88%)	1.4 ± 0.2 (18%)	37 ± 3 (82%)
FeTPP-SCN in DMF (2033 cm^{-1})	0.9 ± 0.2 (23%)	9.0 ± 0.5 (77%)		41 ± 3
NaSCN in DMF		46 ± 3	1.2 ± 0.2 (51%)	5.6 ± 0.5 (49%)

[a]The time constants were determined from the curve fitting using a biexponential function with the expressions of $P_{life} = A_1 \exp(-t/T_1) + A_2 \exp(-t/T_2)$ and $R(t) = B_1 \exp(-t/\tau_1) + B_2 \exp(-t/\tau_2)$. The amplitudes for both the fast and slow components are given in parentheses.

to orientational randomization. Previous studies showed that the rate of vibrational population relaxation should depend on the strength of the coupling to the other modes in the local environments.[42−44] The rotational anisotropy measurements can reveal the overall reorientational dynamics of the global network in the solution. Based on these results, it can be concluded that the SCN ligand with an absorption peak at 2055 cm^{-1} in FeTPP-SCN cannot be simply regarded as the free SCN species. Here, this particular band can be termed as the complex associated species, but different from the bound SCN that connects with the metal center. It should be surrounded by DMF molecules and also is affected by the electrostatic interaction with the metal center in the FeTPP complex. Therefore, the seemingly dissociated SCN ligand is expected to be located in the vicinity of the metal complex, rather than solvated in the bulk of DMF solvents.

The vibrational population relaxation and reorientational dynamics of the bound SCN (2033 cm^{-1}) in FeTPP-SCN were also measured, as shown in Figure 4, parts C and D. Here the 1−2 transition (2008 cm^{-1}) of bound SCN is analyzed to avoid the spectral overlapping with the 1−2 transition of 2055 cm^{-1} band (observed at 2031 cm^{-1}). Detailed analysis of the vibrational population decay resulted in the time constants of 0.9 ± 0.2 ps (23%) and 9.0 ± 0.5 ps (77%). Different from the reorientational dynamics of free SCN ligands, the rotational dynamics of bound SCN can be well described by a single exponential decay with time constant of 41 ± 3 ps. The vibrational energy relaxation of bound SCN is greatly accelerated, mainly due to its direct binding with Fe atom in the complex. The much slower reorientational time constant of the bound SCN indicated that the axial ligand in the complex is strongly confined without any angular restriction, and its

https://doi.org/10.1021/acs.jpclett.2c03235
J. Phys. Chem. Lett. 2022, 13, 11811−11817

orientational relaxation dynamics is correlated with the rotational dynamics of the metal complex as a whole. This is consistent with the slow component of the complex associated SCN in FeTPP-SCN observed in Figure 4B.

We also measured the FTIR spectrum of FeTPP-SCN in the DMSO solution, see Figure S9. There is only one absorption peak in the CN stretching region with a central frequency positioned at 2055 cm^{-1}, which is quite different from the case of the DMF solution. The vibrational lifetime and reorientational time constants of this SCN band are determined to be 65 ± 2 ps and 4.8 ± 0.3 ps, respectively, see Table S3. Based on these measurements, it can be concluded that the axial ligands in FeTPP-SCN complex can be regarded as the free SCN species and should be displaced from the metal center in the DMSO solution.[37] And the polarity of the solvents can have a pronounced effect on the interaction between axial ligand and metal center in the porphyrin complex. This also indicated that the SCN band positioned at 2055 cm^{-1} is not the free species in the DMF solution, and it is expected that the bound SCN and the complex associated SCN species are in equilibrium and are mediated by the electrostatic interaction.

To further elucidate the role of axial ligand in the metal complex during the catalytic activity process, the IR spectra of FeTPP-SCN in DMF solutions under different potentials were measured and shown in Figure S10. It can be found that the bound SCN peak at 2033 cm^{-1} gradually disappeared with the potential scanning from 0.5 to 0 V. This can be understood by the displacement of SCN ligands from the metal center, which is accompanied by the Fe^{III}/Fe^{II} redox process. By further varying the potential from 0 V to −1.4 V, a new peak with absorption frequency at 2076 cm^{-1} can be observed. Control experiment showed that the vibrational frequency of SCN^- interacting with Fe^{2+} in the DMF solution would be observed at 2072 cm^{-1}; see Figure S11. This result confirmed our assumption that the axial ligands of SCN can still be affected during the Fe^{III}/Fe^{II} redox process, rather than dissociated away from the metal center in the complex. When the potential is lower than −1.4 V, only one peak at 2055 cm^{-1} can be observed for FeTPP-SCN in the solution.

Ishitani and co-workers demonstrated that the dissociation of the anionic ligand in rhenium(I) complexes is one of the important processes in the photocatalytic reduction of CO_2.[6,45] They showed that the photocatalytic ability of *fac*-Re(bpy)-$(CO)_3$NCS (Re-NCS) is about twice higher than that of Re−Cl.[45] The elimination of the anionic ligand from the one-electron reduced (OER) species and its recoordination to the Re center after CO generation are both important. They proposed that the balanced properties need to be considered when developing the more efficient photocatalysts for CO_2 reduction based on the rhenium(I) complexes. However, the role of axial ligand for the electrochemical catalytic reduction of CO_2 based on iron porphyrin complex is not explored to the best of our knowledge. Through counteranion exchange from Cl to ClO_4, Masaoka et al. demonstrated that the electrocatalytic activity of FeTPP for CO_2 reduction can be significantly enhanced in MeCN compared with the counterpart in DMF.[19] They showed that FeTPP reacts with CO_2 as Fe^I in MeCN rather than Fe^0 in DMF.[24−26]

In our study, the FeTPP-SCN showed lower electrochemical catalytic activity for the reduction of CO_2 than that of FeTPP-Cl under the same condition. And the reaction center is the reduced species of Fe^0 for both catalysts. Different from the Lehn catalyst, the addition of CO_2 with the active site in FeTPP does not have to be achieved by the elimination of axial ligands. As the CO_2 binding step can be realized through the other side of the planar surface. Therefore, the subtle interaction between the axial ligand and metal center, such as the binding energy and reorganization of surrounding solvents in the vicinity of the complex, can be vital for its electrochemical catalytic activity. From the DFT calculation, the binding energy between Cl and FeTPP (−140.8 kcal/mol) is smaller than that in FeTPP-SCN (−110.2 kcal/mol). The more stable axial ligand coordination in the FeTPP-Cl complex may benefit its electrocatalytic activity. It can be expected that the electron donating property of the axial ligand in the complex and the involved solvent molecules for coordination would be the important factors that controlling its electrochemical performance. The direct link between the orientational dynamics of the axial ligand and the electrocatalytic activity, especially under catalytic conditions by using in situ spectroelectrochemistry warrant further investigation.

In summary, the iron porphyrin complex of FeTPP-SCN is synthesized from a commercially available catalyst of FeTPP-Cl by counteranion exchanging reaction. CV measurements showed that the catalytic activity of FeTPP-SCN is noticeably reduced in DMF solution compared with that of FeTPP-Cl. Linear FTIR measurements showed that there are two types of SCN species in the DMF solutions. Ultrafast IR spectroscopic measurements demonstrated that both the free and bound SCN ligands displayed 3−5 times faster energy redistribution, suggesting that the SCN ligands should be affected by the electrostatic interaction in the FeTPP complex. Rotational anisotropy measurements showed that the reorientational dynamics of SCN ligand was determined to be ∼40 ps, indicating that the ligands are strongly confined and restricted by the global networks formed in the vicinity of metal center. From the electrochemical measurements combined with linear and ultrafast vibrational spectroscopic studies, it was demonstrated that the axial ligands can have a non-negligible effect on the electrocatalytic CO_2 reduction, and the electrochemical catalytic activity can be mediated by the subtle electrostatic interaction between the axial ligands and metal center in the complex.

■ ASSOCIATED CONTENT

Supporting Information

The Supporting Information is available free of charge at https://pubs.acs.org/doi/10.1021/acs.jpclett.2c03235.

Details of synthesis route for FeTPP-SCN, NMR characterization data, and additional electrochemical and IR spectroscopic measurements (PDF)

■ AUTHOR INFORMATION

Corresponding Authors

Hongtao Bian − *Key Laboratory of Applied Surface and Colloid Chemistry, Ministry of Education, School of Chemistry and Chemical Engineering, Shaanxi Normal University, Xi'an 710119, China;* orcid.org/0000-0003-1004-2792; Email: htbian@snnu.edu.cn

Haitao Lei − *Key Laboratory of Applied Surface and Colloid Chemistry, Ministry of Education, School of Chemistry and Chemical Engineering, Shaanxi Normal University, Xi'an 710119, China*; Email: leiht2017@snnu.edu.cn

https://doi.org/10.1021/acs.jpclett.2c03235
J. Phys. Chem. Lett. 2022, 13, 11811−11817

Authors

Jiancong Zheng − *Key Laboratory of Applied Surface and Colloid Chemistry, Ministry of Education, School of Chemistry and Chemical Engineering, Shaanxi Normal University, Xi'an 710119, China*

Dexia Zhou − *Key Laboratory of Applied Surface and Colloid Chemistry, Ministry of Education, School of Chemistry and Chemical Engineering, Shaanxi Normal University, Xi'an 710119, China*

Jinxiu Han − *Key Laboratory of Applied Surface and Colloid Chemistry, Ministry of Education, School of Chemistry and Chemical Engineering, Shaanxi Normal University, Xi'an 710119, China*

Jing Liu − *Key Laboratory of Applied Surface and Colloid Chemistry, Ministry of Education, School of Chemistry and Chemical Engineering, Shaanxi Normal University, Xi'an 710119, China;* orcid.org/0000-0002-8900-4766

Rui Cao − *Key Laboratory of Applied Surface and Colloid Chemistry, Ministry of Education, School of Chemistry and Chemical Engineering, Shaanxi Normal University, Xi'an 710119, China;* orcid.org/0000-0002-1821-9583

Yu Fang − *Key Laboratory of Applied Surface and Colloid Chemistry, Ministry of Education, School of Chemistry and Chemical Engineering, Shaanxi Normal University, Xi'an 710119, China;* orcid.org/0000-0001-8490-8080

Complete contact information is available at: https://pubs.acs.org/10.1021/acs.jpclett.2c03235

Notes

The authors declare no competing financial interest.

■ ACKNOWLEDGMENTS

H.B. acknowledges the support from the Natural Science Foundation of China (NSFC, Nos. 21873062 and 22173054), the Fundamental Research Funds for the Central Universities (GK202001009), and the innovation capability support program of Shaanxi (Program No. 2021TD-18). J.L. acknowledges the support from the Natural Science Foundation of China (NSFC, No. 21972087). H.L. acknowledges the support from the Natural Science Foundation of China (NSFC, No. 21902099) and the Fundamental Research Funds for the Central Universities (GK202103050). We thank Dr. Jingshuang Dang from Shaanxi Normal University for the helpful discussion on the theoretical calculation.

■ REFERENCES

(1) Liang, Z.; Wang, H.-Y.; Zheng, H.; Zhang, W.; Cao, R. Porphyrin-based frameworks for oxygen electrocatalysis and catalytic reduction of carbon dioxide. *Chem. Soc. Rev.* **2021**, *50*, 2540−2581.

(2) Appel, A. M.; Bercaw, J. E.; Bocarsly, A. B.; Dobbek, H.; DuBois, D. L.; Dupuis, M.; Ferry, J. G.; Fujita, E.; Hille, R.; Kenis, P. J. A.; Kerfeld, C. A.; Morris, R. H.; Peden, C. H. F.; Portis, A. R.; Ragsdale, S. W.; Rauchfuss, T. B.; Reek, J. N. H.; Seefeldt, L. C.; Thauer, R. K.; Waldrop, G. L. Frontiers, Opportunities, and Challenges in Biochemical and Chemical Catalysis of CO_2 Fixation. *Chem. Rev.* **2013**, *113*, 6621−6658.

(3) Zhang, S.; Fan, Q.; Xia, R.; Meyer, T. J. CO_2 Reduction: From Homogeneous to Heterogeneous Electrocatalysis. *Acc. Chem. Res.* **2020**, *53*, 255−264.

(4) Costentin, C.; Robert, M.; Savéant, J.-M. Current Issues in Molecular Catalysis Illustrated by Iron Porphyrins as Catalysts of the CO_2-to-CO Electrochemical Conversion. *Acc. Chem. Res.* **2015**, *48*, 2996−3006.

(5) Saha, P.; Amanullah, S.; Dey, A. Selectivity in Electrochemical CO_2 Reduction. *Acc. Chem. Res.* **2022**, *55*, 134−144.

(6) Takeda, H.; Ishitani, O. Development of efficient photocatalytic systems for CO_2 reduction using mononuclear and multinuclear metal complexes based on mechanistic studies. *Coord. Chem. Rev.* **2010**, *254*, 346−354.

(7) Derrick, J. S.; Loipersberger, M.; Chatterjee, R.; Iovan, D. A.; Smith, P. T.; Chakarawet, K.; Yano, J.; Long, J. R.; Head-Gordon, M.; Chang, C. J. Metal−Ligand Cooperativity via Exchange Coupling Promotes Iron- Catalyzed Electrochemical CO_2 Reduction at Low Overpotentials. *J. Am. Chem. Soc.* **2020**, *142*, 20489−20501.

(8) Cometto, C.; Chen, L.; Lo, P.-K.; Guo, Z.; Lau, K.-C.; Anxolabéhère-Mallart, E.; Fave, C.; Lau, T.-C.; Robert, M. Highly Selective Molecular Catalysts for the CO_2-to-CO Electrochemical Conversion at Very Low Overpotential. Contrasting Fe vs Co Quaterpyridine Complexes upon Mechanistic Studies. *ACS Catal.* **2018**, *8*, 3411−3417.

(9) Nie, W.; Tarnopol, D. E.; McCrory, C. C. L. Enhancing a Molecular Electrocatalyst's Activity for CO_2 Reduction by Simultaneously Modulating Three Substituent Effects. *J. Am. Chem. Soc.* **2021**, *143*, 3764−3778.

(10) Nichols, E. M.; Derrick, J. S.; Nistanaki, S. K.; Smith, P. T.; Chang, C. J. Positional effects of second-sphere amide pendants on electrochemical CO_2 reduction catalyzed by iron porphyrins. *Chem. Sci.* **2018**, *9*, 2952−2960.

(11) Margarit, C. G.; Asimow, N. G.; Gonzalez, M. I.; Nocera, D. G. Double Hangman Iron Porphyrin and the Effect of Electrostatic Nonbonding Interactions on Carbon Dioxide Reduction. *J. Phys. Chem. Lett.* **2020**, *11*, 1890−1895.

(12) Gotico, P.; Roupnel, L.; Guillot, R.; Sircoglou, M.; Leibl, W.; Halime, Z.; Aukauloo, A. Atropisomeric Hydrogen Bonding Control for CO_2 Binding and Enhancement of Electrocatalytic Reduction at Iron Porphyrins. *Angew. Chem., Int. Ed.* **2020**, *59*, 22451−22455.

(13) Gotico, P.; Boitrel, B.; Guillot, R.; Sircoglou, M.; Quaranta, A.; Halime, Z.; Leibl, W.; Aukauloo, A. Second-Sphere Biomimetic Multipoint Hydrogen-Bonding Patterns to Boost CO_2 Reduction of Iron Porphyrins. *Angew. Chem., Int. Ed.* **2019**, *58*, 4504−4509.

(14) Mondal, B.; Sen, P.; Rana, A.; Saha, D.; Das, P.; Dey, A. Reduction of CO_2 to CO by an Iron Porphyrin Catalyst in the Presence of Oxygen. *ACS Catal.* **2019**, *9*, 3895−3899.

(15) Azcarate, I.; Costentin, C.; Robert, M.; Savéant, J.-M. Through-Space Charge Interaction Substituent Effects in Molecular Catalysis Leading to the Design of the Most Efficient Catalyst of CO_2-to-CO Electrochemical Conversion. *J. Am. Chem. Soc.* **2016**, *138*, 16639−16644.

(16) Sinha, S.; Warren, J. J. Unexpected Solvent Effect in Electrocatalytic CO_2 to CO Conversion Revealed Using Asymmetric Metalloporphyrins. *Inorg. Chem.* **2018**, *57*, 12650−12656.

(17) Costentin, C.; Passard, G.; Robert, M.; Savéant, J.-M. Pendant Acid−Base Groups in Molecular Catalysts: H-Bond Promoters or Proton Relays? Mechanisms of the Conversion of CO_2 to CO by Electrogenerated Iron(0)Porphyrins Bearing Prepositioned Phenol Functionalities. *J. Am. Chem. Soc.* **2014**, *136*, 11821−11829.

(18) Zhao, B.; Lei, H.; Wang, N.; Xu, G.; Zhang, W.; Cao, R. Underevaluated Solvent Effects in Electrocatalytic CO_2 Reduction by FeIII Chloride Tetrakis(pentafluorophenyl)porphyrin. *Chem. Eur. J.* **2020**, *26*, 4007−4012.

(19) Kosugi, K.; Kondo, M.; Masaoka, S. Quick and Easy Method to Dramatically Improve the Electrochemical CO_2 Reduction Activity of an Iron Porphyrin Complex. *Angew. Chem., Int. Ed.* **2021**, *60*, 22070−22074.

(20) Rury, A. S.; Sension, R. J. Broadband ultrafast transient absorption of iron (III) tetraphenylporphyrin chloride in the condensed phase. *Chem. Phys.* **2013**, *422*, 220−228.

(21) Paulat, F.; Lehnert, N. Detailed Assignment of the Magnetic Circular Dichroism and UV−vis Spectra of Five-Coordinate High-Spin Ferric [Fe(TPP)(Cl)]. *Inorg. Chem.* **2008**, *47*, 4963−4976.

(22) Kadish, K. M.; Bottomley, L. A. Substituent effects on the formation constants of iron(III) and iron(II) tetraphenylporphyrin-pyridine complexes. *J. Am. Chem. Soc.* **1977**, *99*, 2380−2382.
(23) Kadish, K. M.; Larson, G.; Lexa, D.; Momenteau, M. Electrochemical and spectral characterization of the reduction steps of.mu.-oxo-bis(iron tetraphenylporphyrin) dimer in dimethylformamide. *J. Am. Chem. Soc.* **1975**, *97*, 282−288.
(24) Bhugun, I.; Lexa, D.; Savéant, J.-M. Catalysis of the Electrochemical Reduction of Carbon Dioxide by Iron(0) Porphyrins. Synergistic Effect of Lewis Acid Cations. *J. Phys. Chem.* **1996**, *100*, 19981−19985.
(25) Bhugun, I.; Lexa, D.; Savéant, J.-M. Catalysis of the Electrochemical Reduction of Carbon Dioxide by Iron(0) Porphyrins: Synergystic Effect of Weak Brönsted Acids. *J. Am. Chem. Soc.* **1996**, *118*, 1769−1776.
(26) Costentin, C.; Drouet, S.; Passard, G.; Robert, M.; Savéant, J.-M. Proton-Coupled Electron Transfer Cleavage of Heavy-Atom Bonds in Electrocatalytic Processes. Cleavage of a C−O Bond in the Catalyzed Electrochemical Reduction of CO_2. *J. Am. Chem. Soc.* **2013**, *135*, 9023−9031.
(27) Bottomley, L. A.; Kadish, K. M. Counterion and solvent effects on the electrode reactions of iron porphyrins. *Inorg. Chem.* **1981**, *20*, 1348−1357.
(28) Guo, K.; Lei, H.; Li, X.; Zhang, Z.; Wang, Y.; Guo, H.; Zhang, W.; Cao, R. Alkali metal cation effects on electrocatalytic CO_2 reduction with iron porphyrins. *Chinese. J. Catal.* **2021**, *42*, 1439−1444.
(29) Bakker, H. J.; Skinner, J. L. Vibrational Spectroscopy as a Probe of Structure and Dynamics in Liquid Water. *Chem. Rev.* **2010**, *110*, 1498−1517.
(30) Zanni, M. T.; Hochstrasser, R. M. Two-Dimensional Infrared Spectroscopy: A Promising New Method for the Time Resolution of Structures. *Curr. Opin. Struct. Biol.* **2001**, *11*, 516−522.
(31) Hamm, P.; Zanni, M.: *Concepts and Methods of 2D Infrared Spectroscopy*; Cambridge University Press: New York, 2011.
(32) Khalil, M.; Demirdöven, N.; Tokmakoff, A. Coherent 2D IR Spectroscopy: Molecular Structure and Dynamics in Solution. *J. Phys. Chem. A* **2003**, *107*, 5258−5279.
(33) Baiz, C. R.; McRobbie, P. L.; Anna, J. M.; Geva, E.; Kubarych, K. J. Two-Dimensional Infrared Spectroscopy of Metal Carbonyls. *Acc. Chem. Res.* **2009**, *42*, 1395−1404.
(34) Fayer, M. D. Dynamics of Liquids, Molecules, and Proteins Measured with Ultrafast 2D IR Vibrational Echo Chemical Exchange Spectroscopy. *Annu. Rev. Phys. Chem.* **2009**, *60*, 21−38.
(35) Kraack, J. P. Ultrafast Structural Molecular Dynamics Investigated with 2D Infrared Spectroscopy Methods. *Top Curr. Chem.* **2017**, *375*, 86.
(36) Fayer, M. D. Dynamics of Water Interacting with Interfaces, Molecules, and Ions. *Acc. Chem. Res.* **2012**, *45*, 3−14.
(37) Wei, Q.; Zhou, D.; Li, X.; Chen, Y.; Bian, H. Structural Dynamics of Dimethyl Sulfoxide Aqueous Solutions Investigated by Ultrafast Infrared Spectroscopy: Using Thiocyanate Anion as a Local Vibrational Probe. *J. Phys. Chem. B* **2018**, *122*, 12131−12138.
(38) Ohta, K.; Tominaga, K. Vibrational Population Relaxation of Thiocyanate Ion in Polar Solvents Studied by Ultrafast Infrared Spectroscopy. *Chem. Phys. Lett.* **2006**, *429*, 136−140.
(39) Son, H.; Kwon, Y.; Kim, J.; Park, S. Rotational Dynamics of Metal Azide Ion Pairs in Dimethylsulfoxide Solutions. *J. Phys. Chem. B* **2013**, *117*, 2748−2756.
(40) Kinosita, K.; Ikegami, A.; Kawato, S. On the wobbling-in-cone analysis of fluorescence anisotropy decay. *Biophys. J.* **1982**, *37*, 461−464.
(41) Yamada, S. A.; Thompson, W. H.; Fayer, M. D. Water-anion hydrogen bonding dynamics: Ultrafast IR experiments and simulations. *J. Chem. Phys.* **2017**, *146*, 234501.
(42) Bian, H.; Wen, X.; Li, J.; Zheng, J. Mode-specific intermolecular vibrational energy transfer. II. Deuterated water and potassium selenocyanate mixture. *J. Chem. Phys.* **2010**, *133*, No. 034505.
(43) Bian, H.; Chen, H.; Li, J.; Wen, X.; Zheng, J. Nonresonant and Resonant Mode-Specific Intermolecular Vibrational Energy Transfers in Electrolyte Aqueous Solutions. *J. Phys. Chem. A* **2011**, *115*, 11657−11664.
(44) Fenn, E. E.; Wong, D. B.; Fayer, M. D. Water Dynamics at Neutral and Ionic Interfaces. *Proc. Natl. Acad. Sci. U.S.A.* **2009**, *106*, 15243−15248.
(45) Takeda, H.; Koike, K.; Inoue, H.; Ishitani, O. Development of an efficient photocatalytic system for CO_2 reduction using rhenium(l) complexes based on mechanistic studies. *J. Am. Chem. Soc.* **2008**, *130*, 2023−2031.

Recommended by ACS

Redox Behavior of Cobalt–Phosphine Complexes vs Their Catalytic Activity in Organozinc Compound Formation: Background for Mechanistic Investigations
Mykyta O. Ivanytsya, Sergey V. Kolotilov, *et al.*
APRIL 04, 2023
INORGANIC CHEMISTRY
READ

Redox Switching Behavior in Resistive Memory Device Designed Using a Solution-Processable Phenalenyl-Based Co(II) Complex: Experimental and DFT Studies
Nisha Kamboj, Ramesh K. Metre, *et al.*
FEBRUARY 27, 2023
INORGANIC CHEMISTRY
READ

Co(II) Complex with a Covalently Attached Pendent Quinol Selectively Reduces O_2 to H_2O
Segun V. Obisesan, Christian R. Goldsmith, *et al.*
DECEMBER 09, 2022
JOURNAL OF THE AMERICAN CHEMICAL SOCIETY
READ

Manganese Tricarbonyl Diimine Bromide Complexes as Electrocatalysts for Proton Reduction
Wen Liang James Loke, Wai Yip Fan, *et al.*
DECEMBER 09, 2022
INORGANIC CHEMISTRY
READ

Get More Suggestions >

https://doi.org/10.1021/acs.jpclett.2c03235
J. Phys. Chem. Lett. 2022, 13, 11811−11817